# An Indirect Adaptive Approach to Reject Multiple Narrow-Band Disturbances in Hard Disk Drives

Xu Chen and Prof. Masayoshi Tomizuka

UNIVERSITY OF CALIFORNIA, BERKELEY

Emails: maxchen@berkeley.edu, tomizuka@me.berkeley.edu

March 2010

**Abstract**

This report presents an indirect adaptive control scheme that rejects unknown multiple narrow-band disturbance in hard disk drive systems. The proposed algorithm first finds the model of the disturbance (the internal model) and then adaptively estimates its parameters. The design of a band-pass filter with multiple narrow pass-bands is then presented and used to construct a disturbance observer (DOB) for disturbance rejection. The proposed algorithm estimates the minimal amount of parameters, and is computationally simple. Evaluation of the proposed algorithm is performed on a benchmark problem for HDD track following.

# Contents

# List of Figures

# Chapter 1

# Introduction

In track following control of hard disk drives (HDDs), both the repeatable runout (RRO) and the non-repeatable runout (NRRO) contribute to Track Mis-Registration (TMR). RRO is synchronous with the HDD spindle rotation, and can be compensated by customized control algorithms such as adaptive feed-forward cancellation or repetitive control (Sacks et al. (1995)). NRRO, however, differs from track to track, and can appear at frequencies higher than the servo bandwidth (Ehrlich and Curran (1999)). Among the various components in NRRO, disk motion, such as disk fluttering due to turbulent air flow in the hard disk assembly, is the major contributor, and arises as multiple narrow-band disturbances[1] (Guo and Chen (2000); Ehrlich and Curran (1999); McAllister (1996)). With the rapid growth in HDD's storage density, the adverse influence of disk motion on the servo performance is becoming a more and more important issue. Rejection of multiple narrow-band disturbances is thus the key to achieve low TMR in track following.

Investigations of this important problem have been popular in the field of control theory. The existing solutions have mainly been rooted in rejecting disturbance with one narrow-band component. For example, Zheng and Tomizuka (2007, 2008) suggested direct and indirect adaptive disturbance observer (DOB) schemes to estimate and cancel the disturbance; Kim et al. (2005) proposed a parallel add-on peak filter to shape the open loop frequency response; Landau et al. (2005) achieved adaptive narrow-band disturbance rejection on an active suspension, based on

[1] Disturbances whose energy is concentrated at several frequencies.

Youla parametrization. Yet, the problem of *multiple* narrow-band disturbance rejection was seldom examined before. Landau et al. (2005)'s algorithm can be extended to reject $n$ narrow-band disturbances, but requires the estimation of $2n$ parameters.

This report focuses on developing an adaptive control algorithm that rejects any number of unknown narrow-band disturbances in NRRO. The model for multiple narrow-band disturbances, i.e., their internal model, is firstly derived. A new adaptive frequency identification method is then proposed to estimate the parameters of this model, which are then applied to construct a band-pass Q-filter with multiple narrow pass-bands. Finally, expanding the DOB structure in Zheng and Tomizuka (2008) to multiple narrow-band disturbance rejection, we form a disturbance observer with the multiple band-pass Q-filter. Advantages of the proposed compensation scheme are: (1) it estimates the minimal number of parameters, which is equal to $n$, the number of narrow-band components; (2) it is stable over a wide range of frequencies, and disturbances outside the servo bandwidth can also be compensated; (3) it has fast convergence rate, and is easy to implement.

The remainder of this report is organized as follows. Chapter 2 formally defines the problem and introduces the proposed solution. Chapter 3 presents the proposed adaptive frequency identification scheme. The design of DOB with a multiple narrow band-pass Q-filter is shown in chapter 4. An example of rejecting two narrow-band disturbances is provided in chapter 5. Chapter 6 concludes the report.

# Chapter 2

# The Problem And The Proposed Solution

Figure 2.1 shows the block diagram for proposed HDD track following control. It reduces to the baseline feedback control loop if we remove the add-on compensator inside the dash-dotted box. Throughout the report we use the well formulated open-source HDD benchmark problem (Hirata (2007)) as a demonstration tool. The full-order plant model $G_p(z^{-1})$ contains the dynamics of the HDD servo system including the power amplifier, the voice-coil motor, and the actuator mechanics. The dashed line in Fig. 2.2 shows the frequency response of $G_p(z^{-1})$, which is a fourteenth-order transfer function with several high frequency resonances. The baseline feedback controller $C_{FB}(z^{-1})$ is a third order PID controller cascaded with three notch filters. The baseline open loop system has a gain margin of 5.45 dB, a phase margin of 38.2 deg, and an open loop servo bandwidth of 1.19 kHz. The open loop response of the baseline control system is shown in Fig. 2.3.

The reference $r$ is zero in track following control. The signals $d(k)$, $u(k)$, $n(k)$, and $PES$, are respectively the input disturbance, the control input, the output disturbance, and the position error signal. It is assumed that the multiple narrow-band disturbance of interest is contained in $d(k)$, and lies between 300 Hz and 2000 Hz (Guo and Chen (2000); Ehrlich and Curran (1999)).

Figure 2.4 shows the spectrum of the position error signal on one track when the baseline controller is applied. It is observed that several sharp spikes are present due to the multiple narrow-band disturbances, which we aim to reject. The proposed solution is to add a compensator as shown in the dash-dotted box in Fig. 2.1. Within the compensator, the low-order

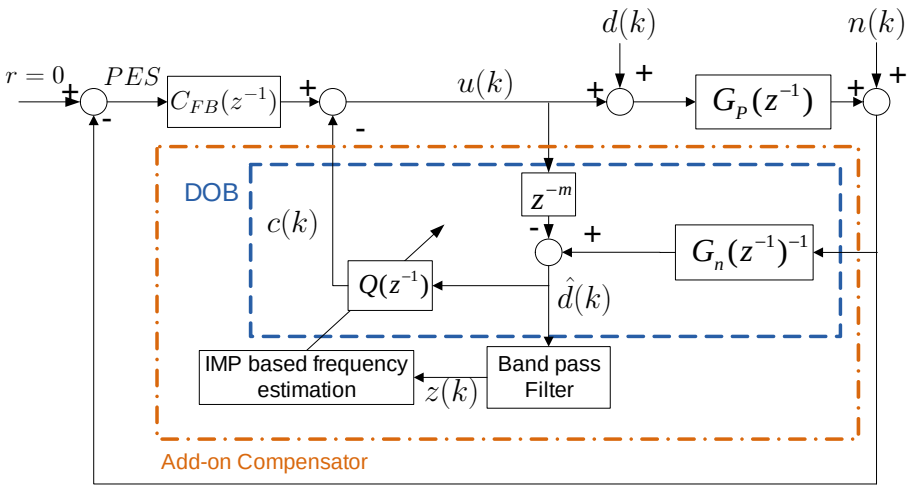


Figure 2.1: Structure of the proposed control scheme.

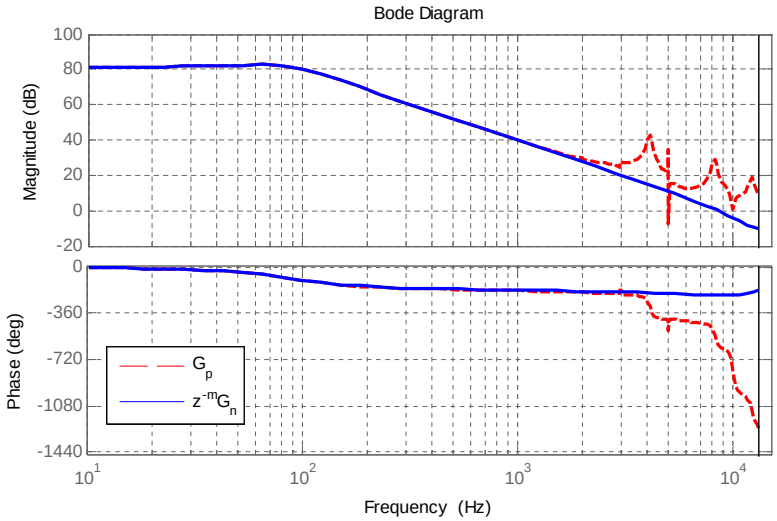


Figure 2.2: Frequency response of $G_p(z^{-1})$ and $z^{-m}G_n(z^{-1})$.

nominal plant model $z^{-m}G_n(z^{-1})$ matches the low-frequency dynamics of $G_p(z^{-1})$ in the frequency response, as shown in Fig. 2.2. A stable inverse model $G_n(z^{-1})^{-1}$ is needed in the design of our proposed compensator. If $G_n(z^{-1})$ has minimal phase, its inverse can directly be assigned, if not, stable inversion techniques such as the ZPET method (Tomizuka (1987)) should be applied.

The compensation signal $c(k)$ is designed, by constructing the DOB, to approximate and cancel the multiple narrow-band disturbances. To see this point, notice first that the signal $\hat{d}(k)$

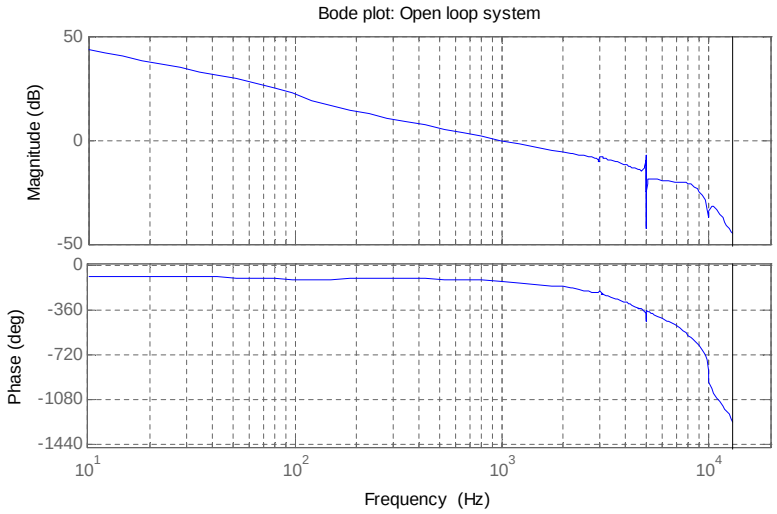


Figure 2.3: Frequency response of the open loop system with the baseline controller $C_{FB}\left(z^{-1}\right)$.

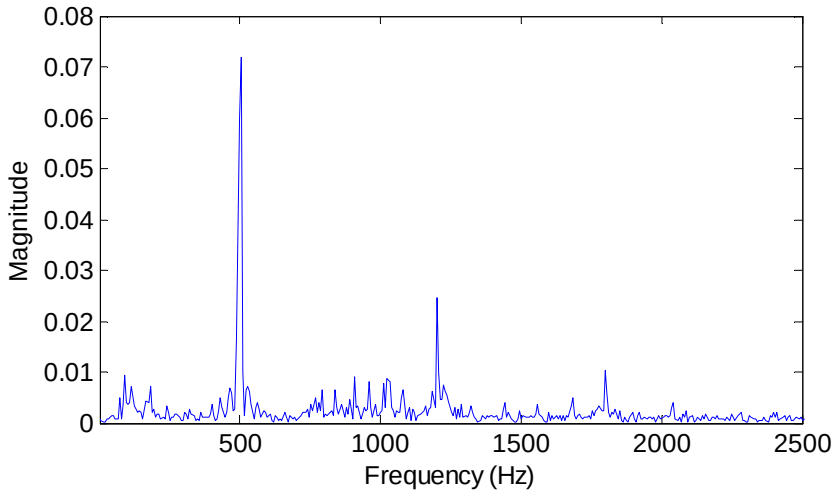


Figure 2.4: PES spectrum with baseline controller.

is expressed by, in the operator notation,

$$\hat{d}\left(k\right)=G_n\left(z^{-1}\right)^{-1}\left[G_p\left(z^{-1}\right)\left(u\left(k\right)+d\left(k\right)\right)+n\left(k\right)\right]-z^{-m}u\left(k\right). \tag{2.1}$$

Since below 2000 Hz, $G_p\left(z^{-1}\right)\approx z^{-m}G_n\left(z^{-1}\right)$, i.e., $G_n\left(z^{-1}\right)^{-1}G_p\left(z^{-1}\right)\approx z^{-m}$, Eq. (2.1) becomes

$$\hat{d}\left(k\right)\approx z^{-m}d\left(k\right)+G_n\left(z^{-1}\right)^{-1}n\left(k\right). \tag{2.2}$$

If in addition the output disturbance $n\left(k\right)$ is small, then the above equation is further

simplified to

$$\hat{d}(k) \approx z^{-m} d(k) = d(k-m), \tag{2.3}$$

which implies that $\hat{d}(k)$ is a good estimate of the disturbance $d(k)$. Therefore, the multiple narrow-band disturbance is contained in $\hat{d}(k)$.

In reality, the influence of $n(k)$ can not be ignored. A band-pass filter $BP(z^{-1})$ is constructed to filter out the signals in $\hat{d}(k)$ that are not of our interest. This is practical since the frequency region of the narrow-band disturbances is usually roughly known. The filtered signal $z(k)$ is finally a multiple narrow-band signal[1] with small noise-to-signal ratio, and can be applied to the parameter estimation scheme to be presented in chapter 3.

With the estimates of the multiple narrow-band disturbances, a multiple band-pass filter $Q(z^{-1})$ can then be constructed. The compensation signal $c(k)$ formed by filtering $\hat{d}(k)$ through $Q(z^{-1})$, therefore contains only the multiple narrow-band disturbance. Adding the negative of $c(k)$ to the control input, we achieve the compensation.

[1]More precisely, $z(k)$ and the multiple narrow-band disturbance in $\hat{d}(k)$ have the same amplitude but different phases.

# Chapter 3

# Adaptive Disturbance Identification

## 3.1 The Internal Model and the Adaptation Algorithm

The multiple narrow-band disturbance in NRRO can be modeled as the sum of several sinusoidal signals (Ehrlich and Curran (1999); Guo and Chen (2000)). It is well known that any sinusoidal signal $x(k)$ satisfies $(1 - 2\cos(\omega) z^{-1} + z^{-2}) x(k) = 0$, where $\omega = 2\pi\Omega T_s$ is the frequency of $x(k)$ in radians[1]. This equality can either be verified by direct expansion or by noting that the zeros of the FIR filter $1 - 2\cos(\omega) z^{-1} + z^{-2}$ lie exactly at $e^{\pm j\omega}$ on the unit circle. The term $1/(1 - 2\cos(\omega) z^{-1} + z^{-2})$ is named as the internal model of $x(k)$.

Assume that the signal $z(k)$ contains $n$ narrow-band components. $z(k)$ will then satisfy

$$\prod_{i=1}^{n} \left(1 - 2\cos(\omega_i) z^{-1} + z^{-2}\right) z(k) = 0, \tag{3.1}$$

where $\omega_i$ $(i = 1, \ldots, n)$ is the frequency of the $i^{th}$ narrow-band component in $z(k)$.

[1] $\Omega$ is the frequency in Hz, $T_s$ is the sampling time in seconds.

The polynomial on the left hand side of Eq. (3.1) is

$$\begin{aligned} A\left(z^{-1}\right) =& \prod_{i=1}^{n}\left(1-2\cos\left(\omega_i\right)z^{-1}+z^{-2}\right) \\ =& 1+a_1z^{-1}+\cdots+a_nz^{-n}+\cdots+a_1z^{-2n+1}+z^{-2n} \\ =& 1+\sum_{i=1}^{n-1}a_i\left(z^{-i}+z^{-2n+i}\right)+a_nz^{-n}+z^{-2n}. \end{aligned} \tag{3.2}$$

The values of $\omega_i's$ are unknown, $a_i's$ are thus unknown, and need to be estimated for constructing $A\left(z^{-1}\right)$. Choosing to directly estimate $a_i's$ makes the adaptation simple in computation, since $A\left(z^{-1}\right)$ is linear in $a_i's$. Notice that the coefficients of $A\left(z^{-1}\right)$ have a mirror symmetric form. Therefore only $n$ parameters need to identified, which is the minimal possible number for $n$ narrow-band signals.

To construct an adaptive estimation scheme, notice that $z\left(k+1\right)$ also satisfies

$$A\left(z^{-1}\right)z\left(k+1\right)=0. \tag{3.3}$$

Substituting and expanding Eq. (3.2) to Eq. (3.3), then moving the terms containing $z\left(k\right)$, $z\left(k-1\right),\ldots,z\left(k+1-2n\right)$ from the left side to the right side, we obtain the adaptation model:

$$z\left(k+1\right)\ =\ -\sum_{i=1}^{n-1}a_i\left[z\left(k+1-i\right)+z\left(k+1-2n+i\right)\right]-a_nz\left(k+1-n\right)-z\left(k+1-2n\right). \tag{3.4}$$

Introduce the parameter vector to be estimated:

$$\theta=\left[a_1,a_2,\ldots,a_n\right]^T. \tag{3.5}$$

Introduce also the regressor vector at time $k$:

$$\phi\left(k\right)=\left[\phi_1\left(k\right),\phi_2\left(k\right),\ldots,\phi_n\left(k\right)\right]^T, \tag{3.6}$$

where

$$\phi_j(k) = -z(k+1-j) - z(k+1-2n+j) \qquad j = 1, ..., n-1 \tag{3.7}$$

$$\phi_n(k) = -z(k+1-n). \tag{3.8}$$

Eq. (3.4) can then be simply represented by

$$z(k+1) = \phi(k)^T \theta - z(k+1-2n). \tag{3.9}$$

We can now define the *a priori* prediction of $z(k+1)$:

$$\hat{z}^o(k+1) = \phi(k)^T \hat{\theta}(k) - z(k+1-2n), \tag{3.10}$$

where $\hat{\theta}(k)$ is the predicted parameter vector at time $k$.

The *a priori* prediction error is given by

$$e^o(k+1) = z(k+1) - \hat{z}^o(k+1) = -\phi(k)^T \tilde{\theta}(k), \tag{3.11}$$

where $\tilde{\theta}(k) = \hat{\theta}(k) - \theta$ is the parameter estimation error.

Correspondingly, we define the following *a posteriori* signals for later use in the stability analysis:

the *a posteriori* prediction of $z(k+1)$:

$$\hat{z}(k+1) = \phi(k)^T \hat{\theta}(k+1) - z(k+1-2n). \tag{3.12}$$

the *a posteriori* prediction error

$$e(k+1) = z(k+1) - \hat{z}(k+1) = -\phi(k)^T \tilde{\theta}(k+1). \tag{3.13}$$

With the above information, the following recursive least squares (RLS) parameter adapta-

tion algorithm (PAA) can be constructed (Landau et al. (1998)).

$$\hat{\theta}(k+1) = \hat{\theta}(k) + \frac{F(k)\phi(k)e^{o}(k+1)}{1+\phi(k)^{T}F(k)\phi(k)} \tag{3.14}$$

$$e^{o}(k+1) = z(k+1) - \hat{z}^{o}(k+1) \tag{3.15}$$

$$\hat{z}^{o}(k+1) = \phi(k)^{T}\hat{\theta}(k) + z(k+1-2n) \tag{3.16}$$

$$F(k+1) = \frac{1}{\lambda(k)}\left[F(k) - \frac{F(k)\phi(k)\phi(k)^{T}F(k)}{\lambda(k)+\phi(k)^{T}F(k)\phi(k)}\right]. \tag{3.17}$$

For the purpose of analysis, Eq. (3.17) can also be written in its inverse form

$$F(k+1)^{-1} = \lambda(k)F(k)^{-1} + \phi(k)\phi(k)^{T}. \tag{3.18}$$

To improve the convergence rate, the forgetting factor $\lambda(k)$ is designed to increase from 0.95 to 1 (Ljung (1999)), obeying the rule

$$\lambda(k) = 1 - 0.05 \times 0.995^{k}. \tag{3.19}$$

.

## 3.2 An Example: the Case of Two Narrow-band Disturbances

In the following, we show the case of $n = 2$ as an example of the parameter estimation algorithm.

Eq. (3.2) now simplifies to

$$A\left(z^{-1}\right) = \left(1 - 2\cos(\omega_1)z^{-1} + z^{-2}\right)\cdot\left(1 - 2\cos(\omega_2)z^{-1} + z^{-2}\right). \tag{3.20}$$

Expanding Eq. (3.20) and introducing

$$a_1 = -2\cos(\omega_1) - 2\cos(\omega_2) \tag{3.21}$$

$$a_2 = 2 + 2\cos(\omega_1) \cdot 2\cos(\omega_2), \tag{3.22}$$

we obtain:

$$A\left(z^{-1}\right) = 1 + a_1 z^{-1} + a_2 z^{-2} + a_1 z^{-3} + z^{-4}. \tag{3.23}$$

The unknown parameter vector is thus given by

$$\theta = \begin{bmatrix} a_1 \\ a_2 \end{bmatrix}. \tag{3.24}$$

The fact that $A(z^{-1})\, z(k+1) = 0$ gives

$$z(k+1) = \phi(k)^T \theta - z(k-3), \tag{3.25}$$

where the regressor vector is given by

$$\phi(k) = \begin{bmatrix} -z(k) - z(k-2) \\ -z(k-1) \end{bmatrix}. \tag{3.26}$$

We can now define the following quantities:

the *a priori* prediction of $z(k+1)$:

$$\hat{z}^o(k+1) = \phi(k)^T \hat{\theta}(k) - z(k-3), \tag{3.27}$$

the *a priori* prediction error:

$$e^o(k+1) = z(k+1) - \hat{z}^o(k+1), \tag{3.28}$$

the *a posteriori* prediction of $z(k+1)$:

$$\hat{z}(k+1) = \phi(k)^T \hat{\theta}(k+1) - z(k-3), \tag{3.29}$$

the *a posteriori* prediction error:

$$e(k+1) \quad = \quad z(k+1) - \hat{z}(k+1), \tag{3.30}$$

The parameter vector $\theta$ can then be estimated according to Eqs. (3.14) through (3.17).

## 3.3 Stability

For stability analysis, we first transform the PAA to the *a posteriori* form. Pre-multiplying $\phi^T(k)$ to Eq. (3.14) yields

$$\phi^T(k)\hat{\theta}(k+1) = \phi^T(k)\hat{\theta}(k) + \frac{\phi^T(k)F(k)\phi(k)}{1+\phi^T(k)F(k)\phi(k)}e^o(k+1). \tag{3.31}$$

Subtracting $\phi^T(k)\theta$ from each side, and substituting Eqs. (3.13) and (3.15) to the resulting expression, we have

$$e(k+1) = \frac{e^o(k+1)}{1+\phi^T(k)F(k)\phi(k)}. \tag{3.32}$$

Substituting the above equation back to Eq. (3.14), we arrive at the PAA in the *a posteriori* form:

$$\hat{\theta}(k+1) = \hat{\theta}(k) + F(k)\phi(k)e(k+1) \tag{3.33}$$

$$e(k+1) = -\phi(k)^T \tilde{\theta}(k+1). \tag{3.34}$$

Subtracting $\theta$ from each side in Eq. (3.33), we obtain

$$\tilde{\theta}(k+1) = \tilde{\theta}(k) + F(k)\phi(k)e(k+1). \tag{3.35}$$

Using Eqs. (3.34) and (3.35), we can construct the equivalent feedback loop for the adaptive system as shown in Fig. 3.1. We then 'add and subtract' a constant 1/2 to the feedback loop, to get the further modified equivalent form in Fig. 3.2.

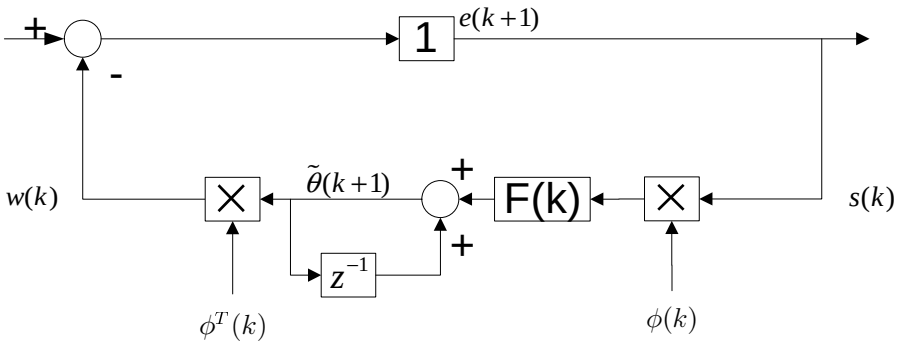


Figure 3.1: Equivalent feedback loop of the adaptive system.

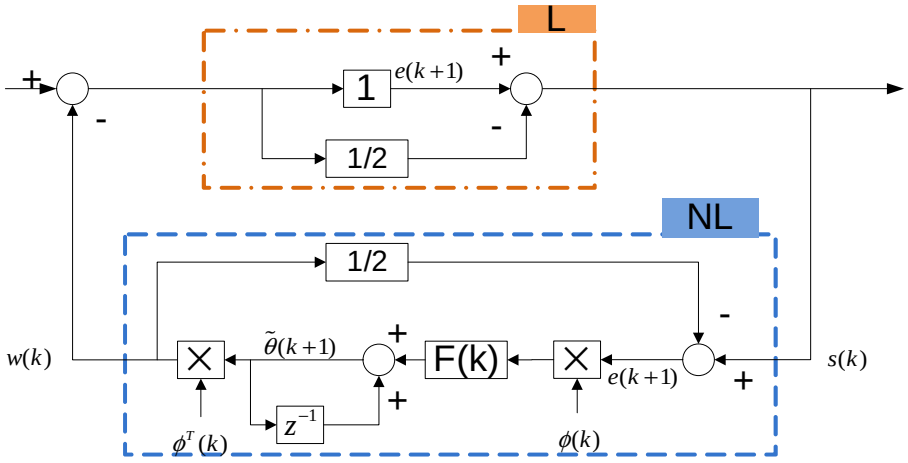


Figure 3.2: A further modified equivalent feedback loop of the adaptive system.

The nonlinear block $NL$ in Fig. 3.2 is passive and satisfies the Popov Inequality (see Appendix A). The linear block $L = 1 - 1/2$ is strictly positive real. Therefore, asymptotic hyperstability of the parameter adaptation algorithm is assured.

## 3.4 Parameter Convergence

Hyperstability of the adaptation algorithm assures the boundedness of the *a posteriori* adaptation error $e(k)$. More specifically, the following inequality holds:

$$|e(k)| < \delta\left(|e(0)| + \gamma\right), \tag{3.36}$$

where $\delta$ and $\gamma$ are positive real numbers.

Notice that in Fig. 3.2, $s(k) = (1 - 1/2)\, e(k+1)$, $w(k) = e(k+1)$. Therefore, the boundedness of $e(k)$ infers that $w(k)$ is bounded.

The convergence of $e(k+1)$ to zero follows from the sufficiency portion of the Asymptotic Hyperstability Theorem and the fact that $w(k)$ is bounded (Landau et al. (1998)).

To see the convergence of the parameters, we note that

$$\lim_{k\to\infty} e(k) = 0. \tag{3.37}$$

Substituting Eq. (3.34) to the above gives

$$\begin{aligned}
&\phi(k-1)^T \tilde{\theta}(k) \\
=&\sum_{i=1}^{n-1} \left(z(k-i) + z(k-2n+i)\right) \tilde{a}_i(k) + z(k-n)\, \tilde{a}_n(k) \\
=&\left(\sum_{i=1}^{n-1} \left(z^{-i} + z^{-2n+i}\right) \tilde{a}_i(k) + z^{-n} \tilde{a}_n(k)\right) z(k) \\
\to&0 \qquad \text{as } k \to \infty.
\end{aligned} \tag{3.38}$$

Based on the assumption that $z(k)$ has $n$ independent frequency components, the Frequency Richness Condition for Parameter Convergence holds. Therefore, the only solution to the above equation is $\lim_{k\to\infty} \tilde{a}_i(k) = 0$, i.e., the parameters converge to their true values.

# Chapter 4

# Multiple Band-pass Q-filter Design

With the estimated parameters in chapter 3, we are ready to design the Q-filter and turn on the adaptive DOB for the disturbance compensation. The Q-filter used in single narrow-band disturbance rejection (Zheng and Tomizuka (2008)) is given by

$$Q\left(z^{-1}\right) = \frac{\left(1-\alpha\right)\left(1-\alpha z^{-2}\right)}{1-\alpha\cdot 2\cos\left(\omega\right)z^{-1}+\alpha^2 z^{-2}}, \tag{4.1}$$

where the shaping coefficient $\alpha$ is a real number close to but smaller than 1. The above Q-filter has two poles close to $e^{\pm j\omega}$ but slightly shifted towards the origin. The magnitude response of $Q\left(z^{-1}\right)$ has a narrow pass-band centered at $\omega$. The closer to 1 the parameter $\alpha$, the narrower the pass-band of $Q\left(z^{-1}\right)$.

For multiple narrow-band disturbance rejection, we extend Eq. (4.1) to

$$Q\left(z^{-1}\right) = \sum_{i=1}^{n} \frac{\left(1-\alpha_i\right)\left(1-\alpha_i z^{-2}\right)}{1-\alpha_i\cdot 2\cos\left(\omega_i\right)z^{-1}+\alpha_i^2 z^{-2}}. \tag{4.2}$$

For simplicity, we let $\alpha_i = \alpha = 0.998$. Recall that $A(z^{-1})$, the denominator of the internal model for multiple narrow-band disturbance, is given by

$$A\left(z^{-1}\right) = \prod_{i=1}^{n}\left(1-2\cos\left(\omega_i\right)z^{-1}+z^{-2}\right) = 1+a_1 z^{-1}+\cdots+a_n z^{-n}+\cdots+a_1 z^{-2n+1}+z^{-2n}. \tag{4.3}$$

Eq. (4.2) can then be expressed as

$$Q\left(z^{-1}\right) = \frac{\left(1-\alpha\right)\left(1-\alpha z^{-2}\right)B_Q\left(z^{-1}\right)}{\prod_{i=1}^{n}\left(1-\alpha\cdot 2\cos\left(\omega_i\right)z^{-1}+\alpha^2 z^{-2}\right)} = \frac{\left(1-\alpha\right)\left(1-\alpha z^{-2}\right)B_Q\left(z^{-1}\right)}{A\left(\alpha z^{-1}\right)}. \tag{4.4}$$

where $A\left(\alpha z^{-1}\right)$ is obtained by replacing every $z^{-1}$ by $\alpha z^{-1}$ in Eq. (4.3), and $B_Q\left(z^{-1}\right)$ is a polynomial of $z^{-1}$.

## 4.1 The Case of Two Narrow-band Disturbances

When $n = 2$, direct expansion in Eq (4.2) gives

$$Q\left(z^{-1}\right) = \frac{\left(1-\alpha\right)\left(1-\alpha z^{-2}\right)\left(2+\alpha a_1 z^{-1}+2\alpha^2 z^{-2}\right)}{1+\alpha a_1 z^{-1}+\alpha^2 a_2 z^{-2}+\alpha^3 a_1 z^{-3}+\alpha^4 z^{-4}}, \tag{4.5}$$

where

$$a_1 = -2\cos\left(\omega_1\right)-2\cos\left(\omega_2\right) \tag{4.6}$$

$$a_2 = 2+2\cos\left(\omega_1\right)\times 2\cos\left(\omega_2\right). \tag{4.7}$$

Notice that $\alpha$, $a_1$ and $a_2$ completely determine $Q\left(z^{-1}\right)$. With the estimated $\hat{a}_1$ and $\hat{a}_2$ in chapter 3, the Q-filter can then be constructed according to Eq. (4.5), which has a frequency response as shown in Fig. 4.1. Notice that at the central frequencies, the magnitude and the phase of $Q\left(z^{-1}\right)$ are 1 (0 dB) and 0 deg, respectively. Therefore, passing a broad band disturbance $\hat{d}\left(k\right)$ through $Q\left(z^{-1}\right)$, one gets the exact multiple narrow-band signals at 500 Hz and 1200 Hz.

The error rejection function $S\left(z^{-1}\right)$ (a.k.a. the sensitivity function), is the transfer function from the output disturbance $n\left(k\right)$ to the position error signal $PES$ in Fig. 4.2. When the DOB

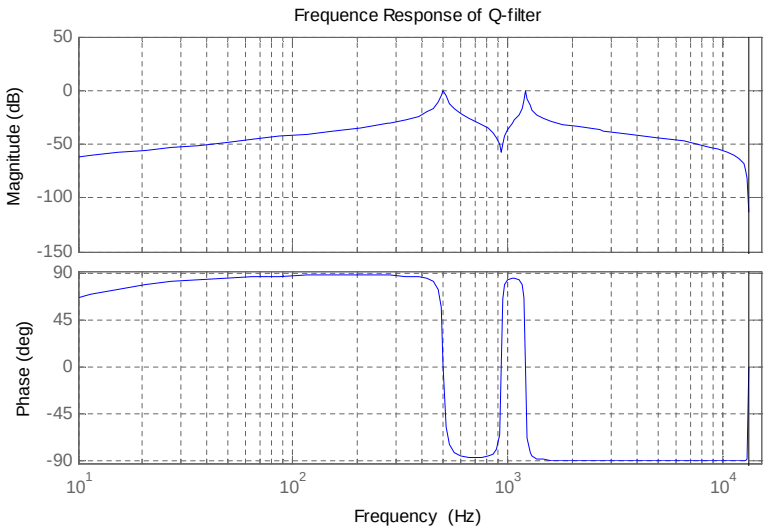


Figure 4.1: Frequency response of the proposed Q-filter (central frequencies: 500 Hz and 1200 Hz).

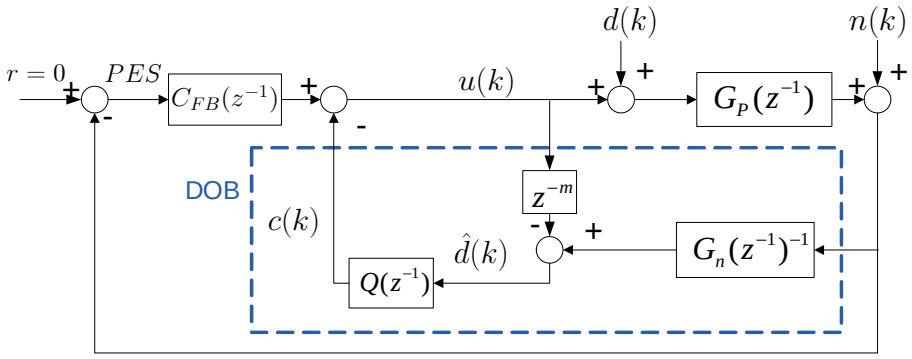


Figure 4.2: Block diagram of the closed loop system with the proposed multiple narrow-band DOB.

is turned on, $S\left(z^{-1}\right)$ can be derived as

$$S\left(z^{-1}\right) = \frac{1}{1 + C_{eq}\left(z^{-1}\right) G_p\left(z^{-1}\right)}, \tag{4.8}$$

where

$$C_{eq}\left(z^{-1}\right) = \frac{G_{FB}\left(z^{-1}\right) + Q\left(z^{-1}\right) G_n\left(z^{-1}\right)^{-1}}{1 - z^{-m} Q\left(z^{-1}\right)}, \tag{4.9}$$

is the equivalent feedback controller.

Figure 4.3 shows the frequency response of the sensitivity function for the closed loop system with the proposed DOB. With the add-on compensation scheme, PES at 500 Hz and 1200 Hz

gets greatly attenuated due to the deep notches in the magnitude response at the corresponding frequencies, while the influence on the sensitivity at other frequencies is negligible.

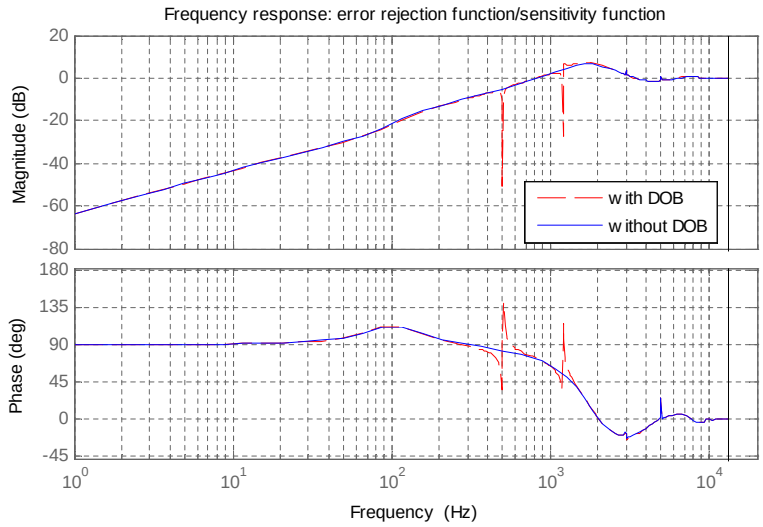


Figure 4.3: Frequency response of the sensitivity function.

Stability of DOB (see Kempf and Kobayashi (1996, 1999)) requires the nominal model $z^{-m}G_n\left(z^{-1}\right)$ to have no zeros outside the unit circle and that

$$\left|Q\left(e^{j\omega}\right)\right| < \frac{1}{\left|\Delta\left(e^{j\omega}\right)\right|}, \quad \forall\omega, \tag{4.10}$$

where

$$\Delta\left(z^{-1}\right) = \frac{G_p\left(z^{-1}\right) - z^{-m}G_n\left(z^{-1}\right)}{z^{-m}G_n\left(z^{-1}\right)} \tag{4.11}$$

is the multiplicative model mismatch. Plotting the magnitude responses of $1/\Delta\left(z^{-1}\right)$ and $Q\left(z^{-1}\right)$ in Fig. 4.4, we see that the multiple narrow-band DOB is stable as long as the narrow-band disturbance arises below 3000 Hz.

## 4.2 The Case of $n$ Narrow-band Disturbances

For the general case of $n$ narrow-band disturbances

$$Q\left(z^{-1}\right) = (1-\alpha)\left(1-\alpha z^{-2}\right)\frac{B_Q\left(z^{-1}\right)}{A\left(\alpha z^{-1}\right)}, \tag{4.12}$$

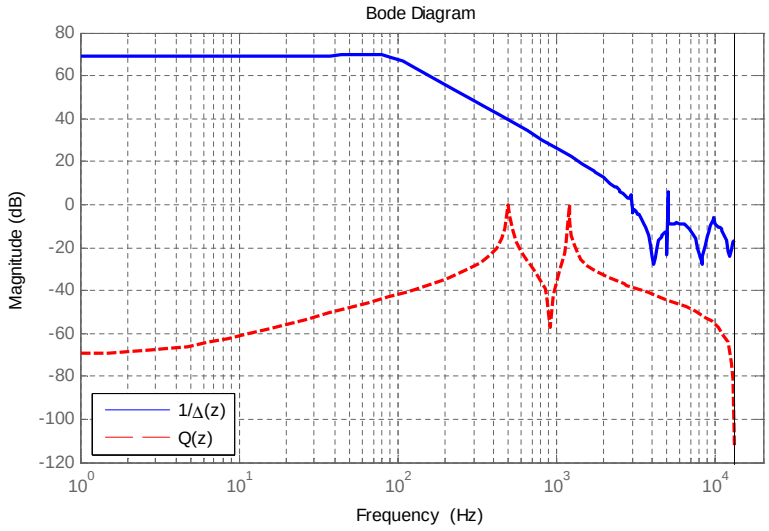


Figure 4.4: Magnitude responses of $1/\Delta\left(z^{-1}\right)$ and $Q\left(z^{-1}\right)$.

where

$$A\left(\alpha z^{-1}\right) = 1 + a_1\alpha z^{-1} + \cdots + a_n\alpha^n z^{-n} + \cdots + a_1\alpha^{2n-1}z^{-2n+1} + \alpha^{2n}z^{-2n}. \tag{4.13}$$

Derivation of the $B_Q\left(z^{-1}\right)$ is best done by using a Computer Algebra System such as *Maple* or *Mathematica*. We have, for $n = 3$,

$$B_Q\left(z^{-1}\right) = 3 + 2\alpha a_1 z^{-1} + \alpha^2\left(a_2 + 3\right)z^{-2} + 2\alpha^3 a_1 z^{-3} + 3\alpha^4 z^{-4}, \tag{4.14}$$

and for $n = 4$,

$$B_Q\left(z^{-1}\right) = 4 + 3\alpha a_1 z^{-1} + \alpha^2\left(2a_2 + 4\right)z^{-2} + \left(a_3 + 3a_1\right)\alpha^3 z^{-3} + \alpha^4\left(2a_2 + 4\right)z^{-4} + 3\alpha^5 a_1 z^{-5} + 4\alpha^6 z^{-6}. \tag{4.15}$$

By induction, we can get the general form of $B_Q\left(z^{-1}\right)$:

$$B_Q\left(z^{-1}\right) = \sum_{i=0}^{n-2} b_i\left(\alpha^i z^{-i} + \alpha^{2(n-1)-i}z^{-2(n-1)+i}\right) + b_{n-1}\alpha^{n-1}z^{-n+1}, \tag{4.16}$$

where

$$b_0 = n$$

$$b_1 = (n-1)\, a_1$$

$$b_i = (n-i)\, a_i + b_{i-2};\ i = 2, \ldots n-1.$$

.

# Chapter 5

# Simulation Results

The proposed adaptive compensator for multiple narrow-band disturbance rejection is implemented in the HDD benchmark problem (Hirata (2007)). The baseline control system is as shown in chapter 2. The disturbances include the torque disturbance, the disk flutter disturbance, the RRO, and the measurement noise. The system has a sampling time of $3.788\times10^{-5}$ sec. Two narrow-band disturbances at 500 Hz and 1200 Hz were injected at the input to the plant.

In the simulated track following, the first five revolutions were run without compensation. It is seen in Fig. 5.1 that the peak values of PES exceeded the standard PES upper-bound of 15% Track Pitch (TP). The dotted line in Fig. 5.2 presents the spectrum of the PES without compensation. We can see that the PES had strong energy components at 500 Hz and 1200 Hz. Without compensation, the Track Mis-Registration (TMR), defined as 3 times the standard deviation of the PES, was 21.87% TP.

The proposed algorithm was applied to improve the HDD track following performance. The multiple band-pass filter $BP\left(z^{-1}\right)$ was designed using the *Signal Processing Toolbox* in *MATLAB*. $BP\left(z^{-1}\right)$ has a magnitude response as shown in Fig. 5.3. The estimation of the parameters was turned on at the beginning of the simulation. The initial guess of the parameter vector was set to half of its true value. Figure 5.4 shows that the estimated parameters $\hat{a}_1$ and $\hat{a}_2$ converged to their true values within one revolution, i.e., 0.0083 sec.

With the estimated parameters $\hat{a}_1$ and $\hat{a}_2$, the Q-filter was constructed and turned on at the

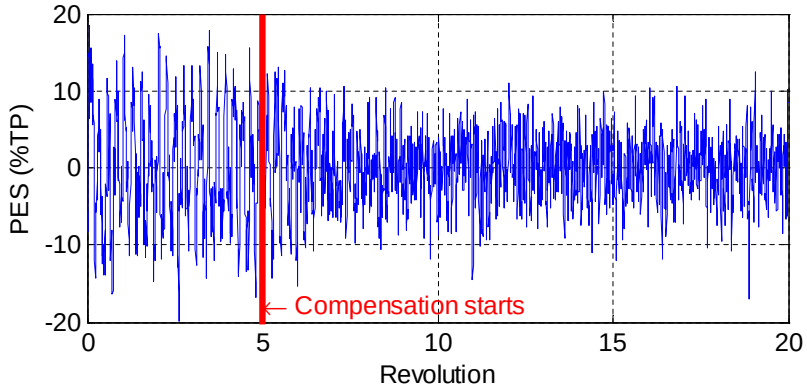


Figure 5.1: PES time trace: compensation starts at the fifth revolution.

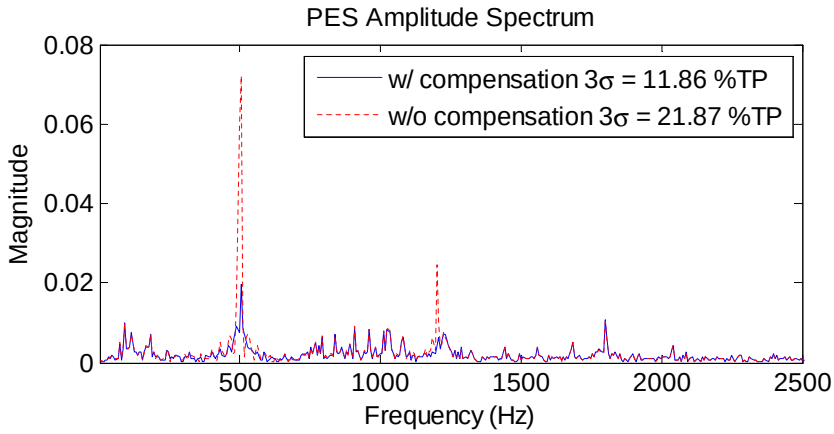


Figure 5.2: PES spectrum with and without the proposed compensator.

fifth revolution. Figure 5.1 shows the resulting PES time trace. It is seen that the PES was reduced now to less than 10% TP. In Fig. 5.2, we observe that the strong energy concentrations at 500 Hz and 1200 Hz were greatly attenuated, while the spectrum of the PES at other frequencies was almost identical to that without compensation. The TMR was reduced to 11.86% TP, implying a 45.8% improvement.

The above simulation has presented validity of the proposed algorithm when the software is coded for $n$ narrow-band signals and the disturbance contains $n$ major frequency components. Convergence of the parameters to their true values is guaranteed in this case, according to the discussion in Section 3.4. When the disturbance contains less than $n$ narrow-band components, there will be multiple solutions to Eq. (3.38). However, stability of PAA is not affected by the frequency richness of its input. The *a posteriori* adaptation error still converges asymptotically to zero in Eq. (3.37). As a result, the model of the multiple narrow-band disturbance is still

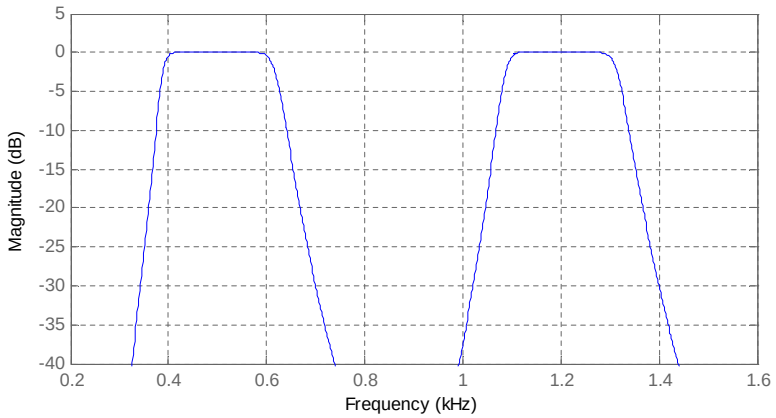


Figure 5.3: Magnitude response of the multiple band-pass filter.

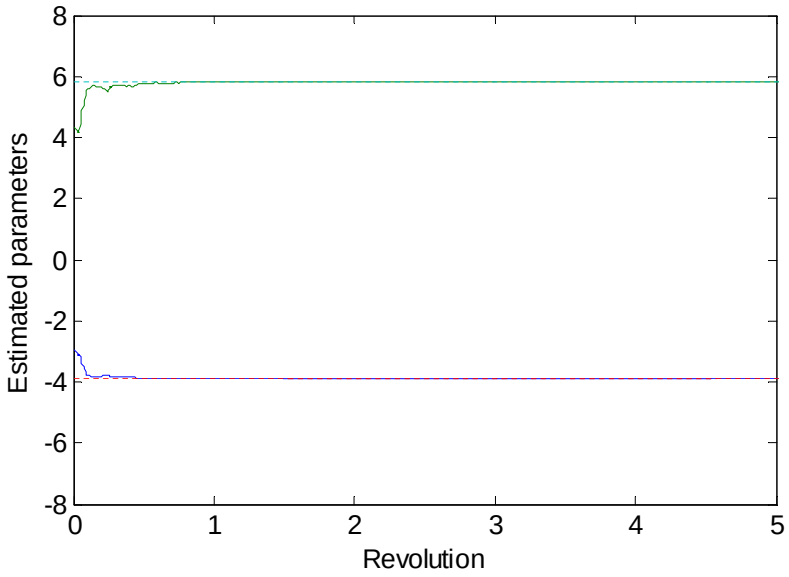


Figure 5.4: Online estimation of the internal model parameters for two narrow-band signals.

captured (in an overdetermined structure, though) by our PAA. To see an example, consider the case that one narrow-band disturbance at 500Hz presents in the HDD system (other disturbances such as sensor noise and torque disturbance are of course still included), but the software is coded to expect two narrow-band components. After obtaining the online parameter estimations $\hat{a}_1$ and $\hat{a}_2$, the estimated frequencies $\hat{\Omega}_1$ and $\hat{\Omega}_2$ can be computed via the following relation:

$$a_1 = -2\cos(\omega_1) - 2\cos(\omega_2) = -2\cos(2\pi\Omega_1 T_s) - 2\cos(2\pi\Omega_2 T_s) \quad (5.1)$$

$$a_2 = 2 + 2\cos(\omega_1) \times 2\cos(\omega_2) = 2 + 2\cos(2\pi\Omega_1 T_s) \times 2\cos(2\pi\Omega_2 T_s)\,. \quad (5.2)$$

Figure 5.5 shows the time trace of $\hat{\Omega}_1$ and $\hat{\Omega}_2$. It is observed that after a transient of less than two revolutions, the 500 Hz frequency is correctly captured by either $\hat{\Omega}_1$ or $\hat{\Omega}_2$. Therefore, compensation of the 500 Hz narrow-band disturbance can still be achieved. In practice, similar to choosing the plant order in system identification, the software should apply as much as possible the a priori information, and choose a value of $n$ that captures all the major disturbance components.

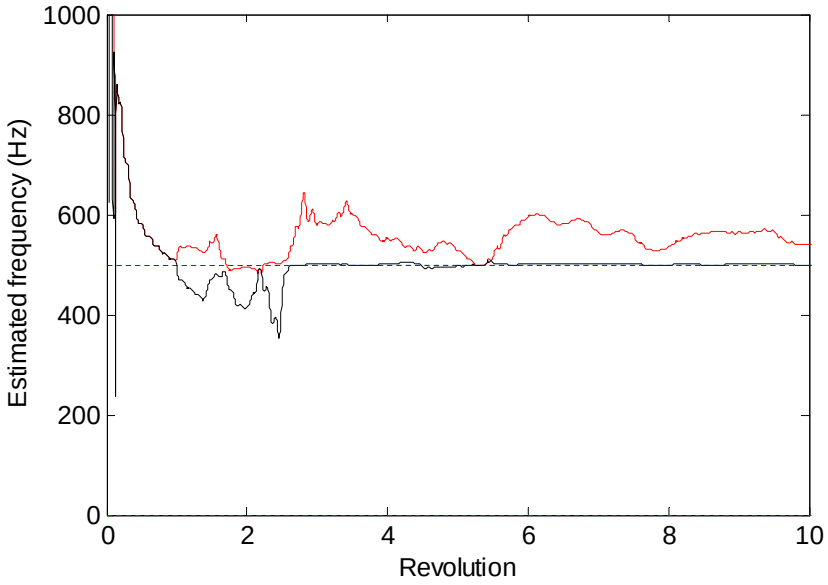


Figure 5.5: Online estimation of the narrow-band frequencies when PAA is designed for two narrow-band signals but the disturbance contains only one major frequency component.

# Chapter 6

# Conclusion

In this report, an indirect adaptive control scheme was proposed to reject unknown multiple narrow-band disturbances in HDD track following. The internal model for arbitrary number of narrow-band disturbances was firstly derived. An adaptive algorithm to identify the unknown frequency information from the internal model was then constructed. The presented algorithm estimates the minimal number of parameters in the internal model, and is computationally efficient. A disturbance observer with a newly designed multiple narrow-bandpass Q-filter was then applied, to estimate and reject the multiple narrow-band disturbance. Simulation on a realistic open-source HDD benchmark problem showed that the proposed algorithm significantly reduced the PES and the TMR.

# Appendix A

# Passivity of the Nonlinear Block in the Adaptive System

Recall the equivalent feedback loop for the adaptive system in Fig. 3.2:

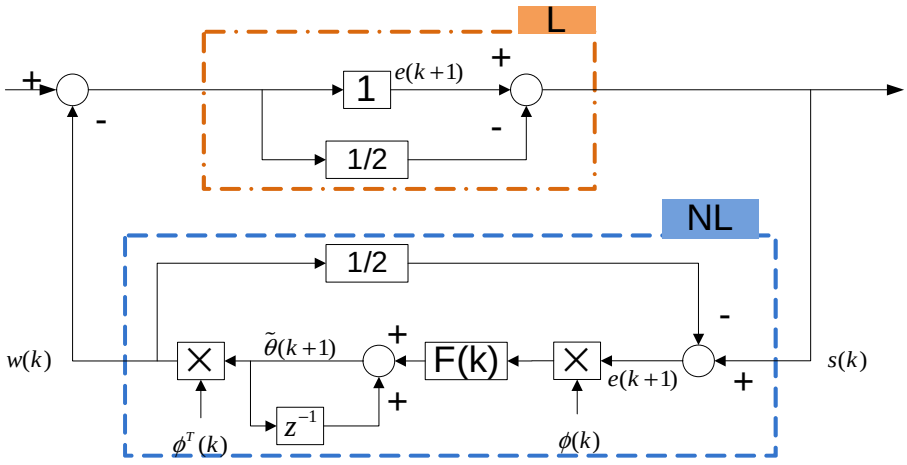


Figure A.1: Equivalent feedback loop of the adaptive system.

For the nonlinear block $NL$ in the above figure, the output $w(k)$ and the input $s(k)$ are given by

$$w(k) = \tilde{\theta}(k+1)^T \phi(k) \tag{A.1}$$

$$s(k) = e(k+1) + \frac{1}{2}\tilde{\theta}(k+1)^T \phi(k) = e(k+1) + \frac{1}{2}\phi(k)^T \tilde{\theta}(k+1). \tag{A.2}$$

To show passivity of the nonlinear block, we consider the inner product of its input and

output:

$$\sum_{k=0}^{k_1} w(k)\, s(k) = \sum_{k=0}^{k_1} \tilde{\theta}(k+1)^T \phi(k) \left[ e(k+1) + \frac{1}{2} \phi(k)^T \tilde{\theta}(k+1) \right]. \tag{A.3}$$

Noting from Eqs. (3.18) and (3.35), that $\tilde{\theta}(k+1) = \tilde{\theta}(k) + F(k)\,\phi(k)\,e(k+1)$ and $F(k+1)^{-1} = \lambda(k) F(k)^{-1} + \phi(k)\,\phi(k)^T$, we have

$$\phi(k)\, e(k+1) = F(k)^{-1} \left( \tilde{\theta}(k+1) - \tilde{\theta}(k) \right) \tag{A.4}$$

$$\phi(k)\,\phi(k)^T = F(k+1)^{-1} - \lambda(k) F(k)^{-1}. \tag{A.5}$$

Substituting the above equations to Eq. (A.3) yields

$$\begin{aligned}
&\sum_{k=0}^{k_1} w(k)\, s(k) \\
=&\sum_{k=0}^{k_1} \left\{ \tilde{\theta}(k+1)^T F(k)^{-1} \left[ \tilde{\theta}(k+1) - \tilde{\theta}(k) \right] + \frac{1}{2} \tilde{\theta}(k+1)^T \left[ F(k+1)^{-1} - \lambda(k) F(k)^{-1} \right] \tilde{\theta}(k+1) \right\}.
\end{aligned}$$

Applying now the identity

$$\tilde{\theta}(k+1)^T F(k)^{-1} \tilde{\theta}(k+1) = \frac{1}{2} \tilde{\theta}(k+1)^T F(k)^{-1} \tilde{\theta}(k+1) + \frac{1}{2} \tilde{\theta}(k+1)^T F(k)^{-1} \tilde{\theta}(k+1),$$

we have

$$\begin{aligned}
&\sum_{k=0}^{k_1} w(k)\, s(k) \\
=&\sum_{k=0}^{k_1} \Bigg\{ \underline{\underline{\frac{1}{2} \tilde{\theta}(k+1)^T \left[ (1 - \lambda(k)) F(k)^{-1} \right] \tilde{\theta}(k+1)}} \\
&\quad + \frac{1}{2} \tilde{\theta}(k+1)^T F(k)^{-1} \tilde{\theta}(k+1) - \frac{1}{2} \tilde{\theta}(k+1)^T F(k)^{-1} \tilde{\theta}(k) \\
&\quad - \frac{1}{2} \tilde{\theta}(k+1)^T F(k)^{-1} \tilde{\theta}(k) + \underline{\frac{1}{2} \tilde{\theta}(k+1)^T F(k+1)^{-1} \tilde{\theta}(k+1)} \\
&\quad + \frac{1}{2} \tilde{\theta}(k)^T F(k)^{-1} \tilde{\theta}(k) \underline{- \frac{1}{2} \tilde{\theta}(k)^T F(k)^{-1} \tilde{\theta}(k)} \Bigg\}.
\end{aligned} \tag{A.6}$$

Combining the underlined terms in Eq. (A.6) gives

$$
\begin{aligned}
&\sum_{k=0}^{k_1} w(k)\, s(k) \\
=&\underbrace{\frac{1}{2}\sum_{k=0}^{k_1} \tilde{\theta}(k+1)^T \left[(1-\lambda(k))\, F(k)^{-1}\right] \tilde{\theta}(k+1)}_{\geq 0} \\
&+\underbrace{\frac{1}{2}\sum_{k=0}^{k_1} \left[\tilde{\theta}(k+1)^T F(k+1)^{-1} \tilde{\theta}(k+1) - \tilde{\theta}(k)^T F(k)^{-1} \tilde{\theta}(k)\right]}_{=\frac{1}{2}\tilde{\theta}(k_1+1)^T F(k_1+1)^{-1}\tilde{\theta}(k_1+1) - \frac{1}{2}\tilde{\theta}(0)^T F(0)^{-1}\tilde{\theta}(0)} \\
&+\underbrace{\frac{1}{2}\sum_{k=0}^{k_1} \left[\tilde{\theta}(k+1)^T F(k)^{-1} \left(\tilde{\theta}(k+1) - \tilde{\theta}(k)\right) - \left(\tilde{\theta}(k+1) - \tilde{\theta}(k)\right)^T F(k)^{-1} \tilde{\theta}(k)\right]}_{=\frac{1}{2}\sum_{k=0}^{k_1}\left(\tilde{\theta}(k+1)-\tilde{\theta}(k)\right)^T F(k)^{-1}\left(\tilde{\theta}(k+1)-\tilde{\theta}(k)\right) \geq 0} \\
\geq&\frac{1}{2}\tilde{\theta}(k_1+1)^T F(k_1+1)^{-1} \tilde{\theta}(k_1+1) - \frac{1}{2}\tilde{\theta}(0)^T F(0)^{-1} \tilde{\theta}(0) \\
\geq&-\underbrace{\frac{1}{2}\tilde{\theta}(0)^T F(0)^{-1} \tilde{\theta}(0)}_{\gamma^2} \qquad \forall k_1 > 0; \quad 0 < \lambda(k) < 1.
\end{aligned} \tag{A.7}
$$

Therefore, the nonlinear block $NL$ satisfies the Popov Inequality, and is thus passive.

# Bibliography

Ehrlich, R., Curran, D., 1999. Major HDD TMR sources and projected scaling with tpi. IEEE Transactions on Magnetics 35 (2), 885–891.

Guo, L., Chen, Y., 2000. Disk flutter and its impact on hdd servo performance. In: Proceedings of 2000 Asia-Pacific Magnetic Recording Conference. pp. TA2/1–TA2/2.

Hirata, M., 2007. NSS benchmark problem of hard disk drive system. http://mizugaki.iis.u-tokyo.ac.jp/nss/.

Kempf, C., Kobayashi, S., 1996. Discrete-time disturbance observer design for systems with time delay. In: Proceedings of 4th International Workshop on Advanced Motion Control. Vol. 1. pp. 332–337.

Kempf, C., Kobayashi, S., 1999. Disturbance observer and feedforward design for a high-speed direct-drive positioning table. IEEE Transactions on Control Systems Technology 7 (5), 513–526.

Kim, Y., Kang, C., Tomizuka, M., 2005. Adaptive and optimal rejection of non-repeatable disturbance in hard disk drives. In: Proceedings of 2005 IEEE/ASME International Conference on Advanced Intelligent Mechatronics. Vol. 1. pp. 1–6.

Landau, I. D., Constantinescu, A., Rey, D., Apr. 2005. Adaptive narrow band disturbance rejection applied to an active suspension–an internal model principle approach. Automatica 41 (4), 563–574.

Landau, I. D., Lozano, R., M'Saad, M., 1998. Adaptive Control. Springer-Verlag New York, Inc.

Ljung, L., 1999. System Identification: Theory for the User, 2nd Edition. Prentice Hall PTR.

McAllister, J., May 1996. The effect of disk platter resonances on track misregistration in 3.5 inch disk drives. IEEE Transactions on Magnetics 32 (3), 1762–1766.

Sacks, A., Bodson, M., Messner, W., 1995. Advanced methods for repeatable runout compensation disc drives. IEEE Transactions on Magnetics 31 (2), 1031–1036.

Tomizuka, M., 1987. Zero phase error tracking algorithm for digital control. Journal of Dynamic Systems, Measurement, and Control 109 (1), 65–68.

Zheng, Q., Tomizuka, M., 2007. Compensation of dominant frequency components of nonrepeatable disturbance in hard disk drives. IEEE Transactions on Magnetics 43 (9), 3756–3762.

Zheng, Q., Tomizuka, M., 2008. A disturbance observer approach to detecting and rejecting narrow-band disturbances in hard disk drives. In: Proceedings of 2008 IEEE International Workshop on Advanced Motion Control. pp. 254–259.